Solid Freeform Fabrication 2023: Proceedings of the 34th Annual International Solid Freeform Fabrication Symposium – An Additive Manufacturing Conference
Reviewed Paper

PARAMETRIC ANALYSIS OF DEPOSITION PRESSURE CONTROLLED MULTI-AXIS FREE-FORM FABRICATION

N. Kyriazis*, J. Eine*, and A. R. Thakur*‡
*Institute of Space Systems, Technical University of Braunschweig, 38108 Braunschweig, Germany.
‡Corresponding author: aditya.thakur@tu-braunschweig.de

Abstract

Additive manufacturing is being explored as one of the most promising in-space manufacturing techniques. The presence of micro-gravity enables the fabrication of support-free sparse structures with ease. Sparse lattice structures (e.g. trusses) are attractive for space applications as they can be tailored for specific load paths. Previous studies have identified a positive correlation between deposition pressure and inter-layer adhesion in 3D printing. However, excessive deposition pressures negatively influence the in-orbit printing accuracy. Therefore, a parametric investigation was conducted to determine the optimal deposition pressure to fabricate mechanically sound trusses in orbit. Support-free arches with varying nodal deposition pressures were 3D printed using a multi-axis robotic manipulator with integrated force sensors. Mechanical testing of these arches concluded that the strength improvement plateaus and registers no significant increase in (joint) strength after a certain deposition pressure, characterized by the properties of the extrude. Integration of a force-feedback facilitates free-form printing of complex, multi-layered, support-free structures in terrestrial environments. In a free-floating space environment, it assists in optimizing the overall printing process.

Nomenclature and Abbreviations

AM	Additive Manufacturing
DoF	Degrees of Freedom
ELISSA	Experimental Lab for Proximity Operations and Space Situational Awareness
FFF	Fused Filament Fabrication
ISM	In-space Manufacturing
ISS	International Space Station
PEEK	Polyether Ether Ketone
PEKK	Polyether Ketone Ketone
PEI	Polyetherimide
PLA	Polylactic Acid
ROS	Robot Operating System

Introduction

A common practice in the development of space structures is to build and test them on the ground and then transport them into orbit as a payload in a launch vehicle. Thus, the structure must be designed in such a way that it can withstand the launch loads. Since these launch loads are usually much higher than the loads during actual orbital operations, the structure is often excessively reinforced and therefore ends up being much heavier than is required for the in-orbit operations alone. Additionally, the limited stowage space of the rocket defines the size of the object to be transported. This limitation is currently being circumvented via deployable folding mechanisms. Consequently, this increases the complexity of the overall system, contributing to an increased probability of failure [1, 2].

The possibility of manufacturing such structures directly in space would counteract these issues and enable the manufacturing of much larger structures. However, this creates new challenges and difficulties that are required to be addressed. Although additive manufacturing (AM) methods have already been successfully tested

under micro-gravity conditions on the International Space Station (ISS) [3, 4, 5, 6], some issues remain unresolved, viz. production of large load-bearing structures such as trusses in space.

Support-free, free-form fabrication is especially attractive for in-space manufacturing (ISM) with micro-gravity facilitating the printing process without requiring any additional support material. Thus, improving the resource efficiency of the overall process, and consequently minimizing its impact on the space debris environment. A variety of different approaches have already been investigated to reduce (or even eliminate) the use of support material in AM. Some examples include the use of a rotating cuboidal base that allows intermittent printing of multiple partitioned geometries with reduced reliance on support materials [7], introducing tilt to the printing substrate with a Stewart mechanism [8], and using a robotic arm [9, 10] simply to increase the degrees of freedom (DoF) while printing. For large-format ISM, such approaches with substrate manipulations are usually impractical. Hence, a novel approach must devise to 3D print without any support material.

One possible way to large-format AM without any support material can be via the free-hanging 3D printing approach [11]. The feasibility of adapting this approach for ISM has already been assessed [12, 13, 14]. Using a standard thermoplastic extruder with a robotic manipulator coordinated with a free-flying satellite, meter-scale support-free trusses were printed with sub-millimeter accuracy in a space simulated-environment. Combining the free-hanging 3D printing approach with a mobile free-flying platform allows structures to be printed that are much larger than the range of motion of the robotic manipulator.

Manufacturing structures in a free-flying environment comes with many challenges. The interaction of the extruded material with the substrate during the printing process results in a reaction force due to friction. The absence of any dampening to this feedback negatively affects the printing accuracy as the position of the free-flyer is disturbed (See Fig. 1). The design of the current setup with the robotic arm extending beyond the satellite module exacerbates the reaction forces and amplifies the position errors resulting from the printing process [13].

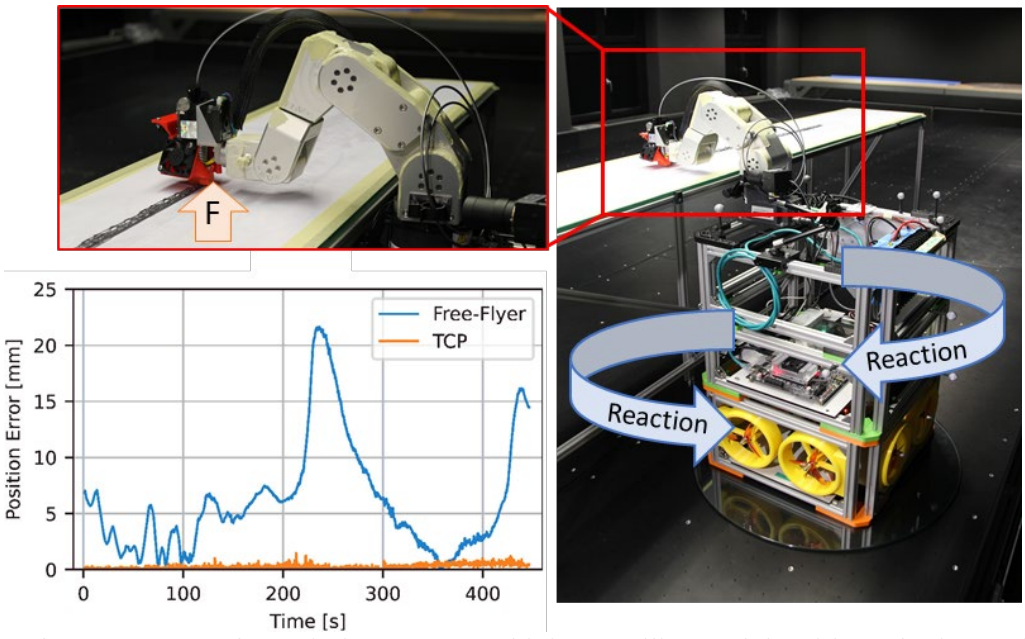

Fig. 1. Large format, support-free printing setup combining satellite module with a robotic arm in ELISSA environment. The free-flying setup is particularly susceptible to disturbances with small position errors at the tool center point (TCP) due to friction causing large reactionary position errors in the free-flying satellite.

In [12, 13] it has already been demonstrated that the printing of free-hanging truss structures in such conditions is possible via robust station-keeping algorithms. However, these algorithms through low-pass filters may overcompensate the disturbances, compromising the trajectory and consequently, the overall printability

[13]. An integrated sensor capable of detecting the forces during the printing process may assist in complementing the existing printing algorithms to minimize this disturbance-induced error without compromising the printing process.

In sparse lattice structures, joints present a particularly weak point. Especially in structures produced using the freeform AM processes, due to the limited contact area at the joints, the structure is at its weakest. In conventional layer-by-layer AM, this weakness is mitigated as the contact area extends across the entire cross-section of the deposition. Yet, for unidirectional structures, inter-layer strength is comparatively weak. This is further exaggerated within support-free lattice structures manufactured using a free-hanging printing approach. Since joint failure is usually the cause of lattice structure failure, it is necessary to determine manufacturing solutions to improve joint strength within such structures. One of the identified approaches to achieve this strength improvement is by increasing the applied pressure at the joints during the printing process. Previous studies have explored the use of a heated pressure rollers to enhance the properties of 3D printed parts [15]. However, the use of such apparatus is impractical for free-form support-free printing.

In this study, by integrating a force sensor in the multi-axis robotic manipulator, we conduct a parametric study by varying the deposition pressure during the support-free AM of trusses. The impact of deposition pressure on the joint strength was systematically studied to facilitate 3D printing of multilayered trusses with elevated mechanical strength for terrestrial printing applications. For ISM, this force feedback assists in optimizing the free-flying printing process by limiting the need for dampening algorithms, by reducing the impact of interaction between the extruded material and the substrate.

Experimental Setup

The path to an on-orbit 3D printer, which is capable of printing functional complex structures is long and requires several intermediate steps. Currently, the experiments are being conducted in the Experimental Laboratory for Proximity Operations and Space Situational Awareness (ELISSA) at the Technical University of Braunschweig (Germany) to establish the feasibility of the concept. ELISSA comprises of an active air bearing table that emulates weightlessness and in-orbit contact dynamics. It is complemented by a low latency, high precision 6DoF motion capture optical tracking system. A space-simulated friction-less planar (3DoF) motion is thus facilitated in an ambient environmental condition. A satellite mock-up equipped with a robotic manipulator with a fused filament fabrication (FFF) end effector is used. This setup is employed to optimize support-free large-format AM process in a high-fidelity test environment simulating on orbit free-flying conditions (See Fig. 2 a). For preliminary analyses and developing novel approaches to optimize printing with an integrated force sensor, the robotic manipulator subsystem was investigated separately, before again integrating it into the existing satellite printing setup.

Robotic Manipulator-based 3D Printing Setup

A commercial robotic arm UR3[1] with a direct-drive FFF print setup mounted to it was used to AM support-free structures. The FFF print head consists of a Titan extruder, a 24V SuperVolcano heater with a corresponding 1.4 mm brass nozzle, and a V6 universal heat sink with corresponding cooling by E3D[2]. All parts are connected to the robot arm by a specially designed bracket, which also incorporates multiple fans for cooling the printed parts (See Fig. 2 b). Due to its low cost, low printing temperature, and easy handling, Polylactic acid (PLA) is used as the printing material in the parametric study. It must be noted that PLA is not intended for operations in space due to its low-temperature resistance and strength. Instead, space-compatible engineering thermoplastics like PEEK, PEKK, and PEI, which are compatible with the FFF process, are recommended [14].

[1] Universal Robots GmbH, Denmark.
[2] E3D, United Kingdom.

A three-axis force sensor K3D40[3] is integrated within the interface between the robot arm and the print head to measure the vertical forces. This information is then processed to determine the deposition pressure during the printing process. This pressure information is then used as an input variable for a control system to systematically apply desired nodal pressure within the printed support-free trusses.

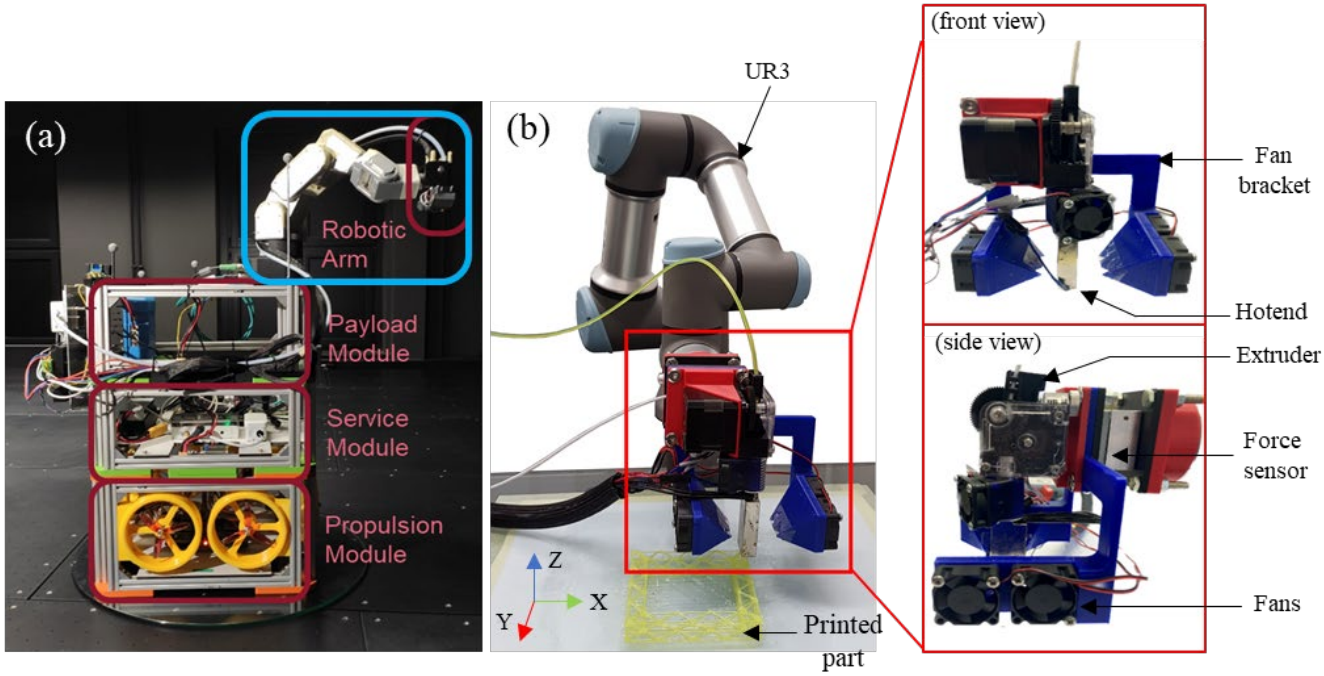

Fig. 2. (a) ELISSA-based mobile satellite module equipped with robotic manipulator and FFF printer setup (highlighted in blue); (b) stationary robotic arm with an integrated force sensor, customized cooling bracket, and FFF printer setup.

To ensure communication and control of all the subsystems, the Robotic Operating System (ROS) is used. The printing process is enabled via G-code which is analyzed by a customized parser that converts the information it contains into a format that is routed to the subsystems via ROS. For pressure-controlled printing, certain modifications were made to the system. Therefore, two separate G-code commands are defined, which are needed for the control of the force sensor.

The force-controlled joint command executes a movement in the negative z-direction until a defined force is reached and the tare command tares the force sensor. For the parser to interpret the G-code, it must be extended with corresponding reading functions. In the program sequence, a loop verifies whether the new command (G122) is contained. If this is the case, the argument of the command is read in, which contains the specified force. This is subsequently compared in a loop with the measured force from the force sensor. If the measured force is lower than the specified force, the print head is lowered (by 0.5 mm for the current setup). The loop is terminated when the desired force is achieved or if the safety distance is exceeded. The schematic sequence of the program is shown in Fig. 3.

[3] ME- Meßsysteme GmbH, Germany.

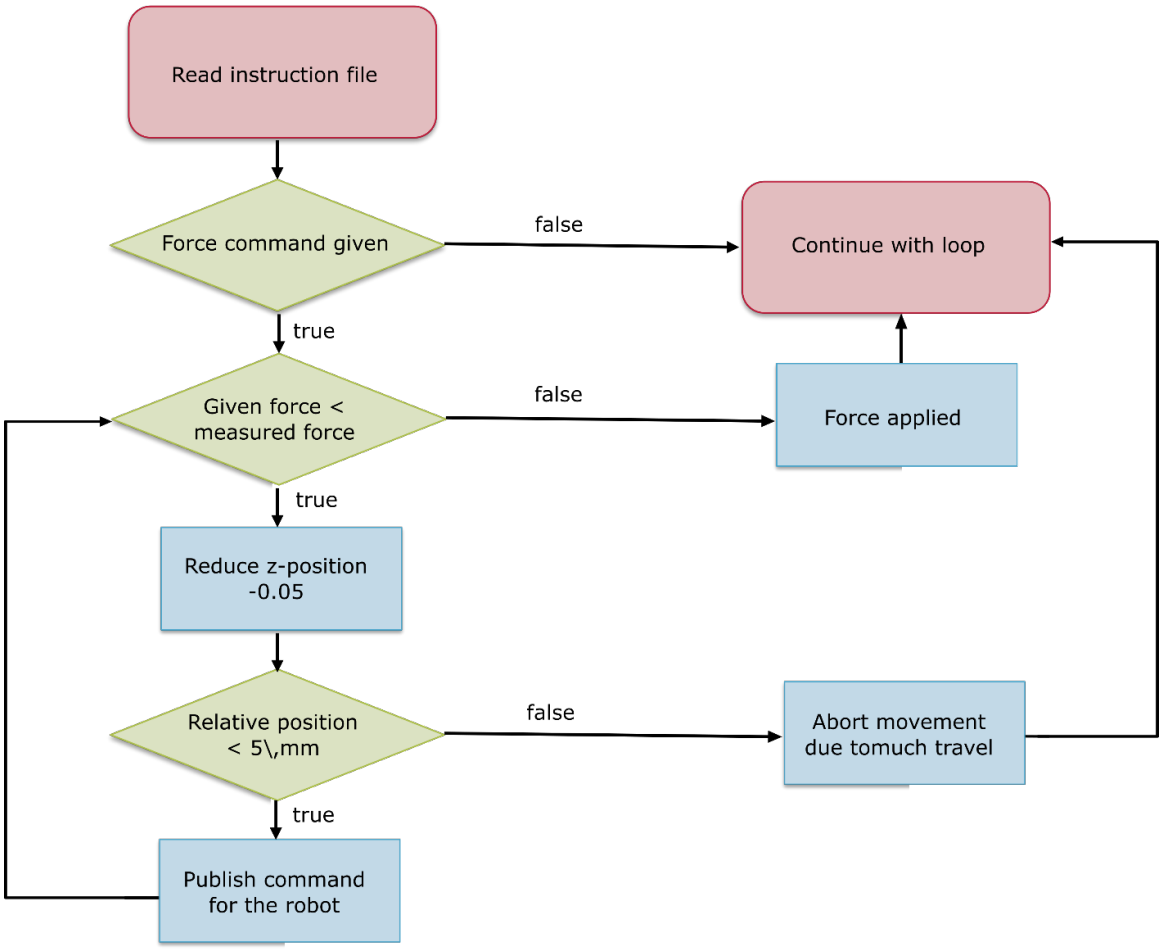

Fig 3. Logical flowchart of the working principle of the program that controls the applied force using the force sensor

Free-form Fabrication Process

Due to the different conditions in space compared to those on Earth, AM using the FFF process must consider aspects that do not arise while printing on Earth. For example, the molten thermoplastics behave differently in a vacuum, heat dissipation is primarily via radiation, etc. However, not all altered conditions need to be insurmountable obstacles. They can also present opportunities to implement printing processes that are not easily possible on Earth. Micro-gravity, for instance, facilitates flexible and efficient printing of support-free structures. Although such a printing process already exists with free-form fabrication, it mandates self-supporting or overhanging structures to be extruded for terrestrial applications due to gravity. Liu et al. [11] proposed an adjustment of the printing trajectory that considers the thermal properties of the printed filament and the printing speed to determine the stretch of the printed filament that is deformable. This allows for the determination of how much the filament will sag under the influence of gravity, using which a corresponding compensation trajectory can be calculated. The modified compensation trajectory method is also employed in this presented study to create lattice structures in the space-simulated testing environment of ELISSA as well as with separated subsystem assessment using the robotic manipulator. A schematic representation of the free-form printing of the lateral structure within the lattice is shown in Fig. 4.

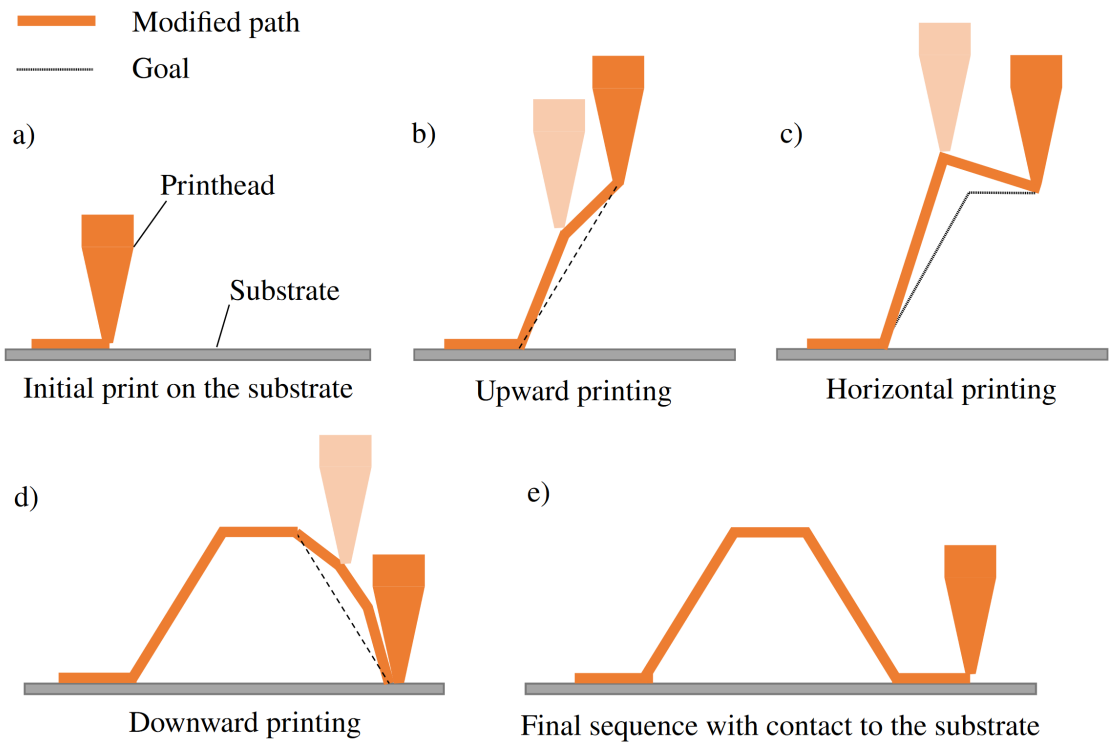

Fig. 4. Schematic illustration of support-free free-form fabrication principle with (a) initial print phase interaction between substrate and deposition, (b) adapted upward printing trajectory, (c) horizontal printing trajectory, and (d) downward printing trajectory accounting for the final print geometry and material solidification rate, concluding with (e) final sequence adhering deposition back onto the substrate.

The optimal shape for the desired lateral structure is a trapezoid. To achieve this, the fabrication process can be divided into three sections: the upward section, the horizontal section, and the downward section. In the upward section (Fig. 4 b), the printing trajectory is inclined at an angle α higher than the target structure. This angle is tallied accounting for the free-hanging material behavior upon being extruded from the nozzle (32°for the current print). For the horizontal section (Fig. 4 b), the trajectory runs linearly from the endpoint of the upward section to the corner point of the desired trapezoidal shape. Since the total distance covered by the trajectory is longer than the length of the trapezoid, it is necessary to prevent excessive material extrusion. Therefore, an extrusion pause is introduced at the beginning of the horizontal section to interrupt the extrusion ensuring that just an adequate amount of filament is extruded. The malleable extruded material is thus shaped into the correct form at the beginning of the horizontal section. Similarly, for the downward section (Fig. 4 c), the trajectory is adjusted at the intermediate target point located halfway along the horizontal coordinates to print the desired trapezoid. The extrusion rate is moderated accordingly.

In addition to the trajectory, printing parameters also play a significant role. Using a lower nozzle temperature along with improved deposition cooling quickens solidification and promotes printability without requiring support materials. Modifying the printing speed to match the curing rate of the material ensures that the material solidifies at the intended position and orientation defined by the trajectory of the nozzle. For the illustrated truss-printing process, the printing temperature of 150°C was used to manufacture PLA trusses. A customized cooling setup was devised to simultaneously direct the flow of air from four cooling fans onto the extruded deposition (See Fig. 2 b). The printing speed of 120 mm/min was used for the material extrusion rate of 80 %.

Testing Procedure

Trusses have been identified as key structures for ISM for being resource efficient, easy to manufacture, and yet being simultaneously functional for space applications [12]. They are typically employed as load-bearing structures. Therefore, the strength of the truss, which is often dictated by the strength of the joints between its elements, determines its final application. Previous investigations have successfully enabled the printing of large-format support-free trusses in a space-simulated environment within ELISSA [12, 14]. However, during this feasibility assessment, it was observed that the friction forces between the extrude and the substrate lead to the reaction forces that are detrimental to 3D printing within the free-flying environment using a satellite as a mobile printing platform. Thus, negligibly low deposition pressure was used to fabricate truss structures. As a result, a thorough parametric study had to be conducted to correlate the reaction forces generated during the free form printing, its effect on the printability, and the strength of the printed sparse structures. Higher deposition pressure ensures improved joint strength. However, the resulting reaction forces negatively affect the stability of the mobile printing platform. To optimize the printed truss structure without compromising its printability, a systematic parametric test was conducted. Combining the free-form fabrication procedure, using the robotic manipulator-based printing setup and the deposition pressure algorithm, as illustrated in Fig. 4, Fig. 2, and Fig. 3, respectively, test specimens with varying deposition pressures were manufactured.

Tensile tests on the joints produced using different contact pressures were conducted. Generally, to test tensile strength, the ASTM D638 standard is suitable using a dog-bone structure. However, since only the joints within the trusses are to be tested, the specified dog-bone geometry is not practical. On the other hand, the ASTM D7249 standard which is used to test the sandwich constructions using 3-point bending tests can be adapted for the 3D printed lattice structures. However, due to unwanted confounding factors like the outer layers and the connection between the lattice and the shell, this testing approach is not suitable for the current 3D printed truss structures. Therefore, it was necessary to consider a novel alternate testing approach that specifically evaluates the strength of the joints in relation to the deposition pressure. This was achieved by designing and fabricating customized joint specimens that isolate the joint area for testing under controlled conditions.

Instead of testing the entire lattice truss structure, only a side arch is tested. This arch is printed onto a base plate and then subjected to tension. The test specimen is illustrated in Fig. 5. The specimens consist of a 2D base plate measuring 24 mm x 60 mm. The base plate improves stability and securely clamps in the testing machine. Near the base, it serves the same purpose as the 1D filament used as the foundation in lattice truss structures. The base plate is 1.8 mm thick, providing sufficient rigidity and stability to exclude it as the failure location. On top of the base plate, an arch with a height of 10 mm and a span of 25 mm is 3D printed using the free-form fabrication manufacturing process as illustrated in Fig. 4. The two connection points between the arch and the base plate are created using the nodal deposition pressure method, as illustrated in Fig. 5 a. The arches are printed with different prescribed contact forces of 0, 2, 4, 6, 8, 10, and 12 Newtons. Concurrently, the force applied during the printing process is recorded to determine the actual deposition pressure applied. Five specimens were fabricated and tested for each deposition pressure value (See Fig. 5 b). By testing these specially designed arch specimens, the focus is solely on assessing the strength of the joints, without the interference of other factors. This approach allows for a targeted investigation into the relationship between joint strength and deposition pressure. Thus, providing valuable insight into the optimized printing of lattice truss structures, for terrestrial as well as space applications.

The specimens are tested using an applied tensile load, following the guidelines of ASTM D638, except for the sample geometry. A strain rate of 5mm/min is used to ensure that the tests can be considered quasi-static. The accuracy requirements for the sensors and components are also based on the testing standards, using standard tensile testing machines.

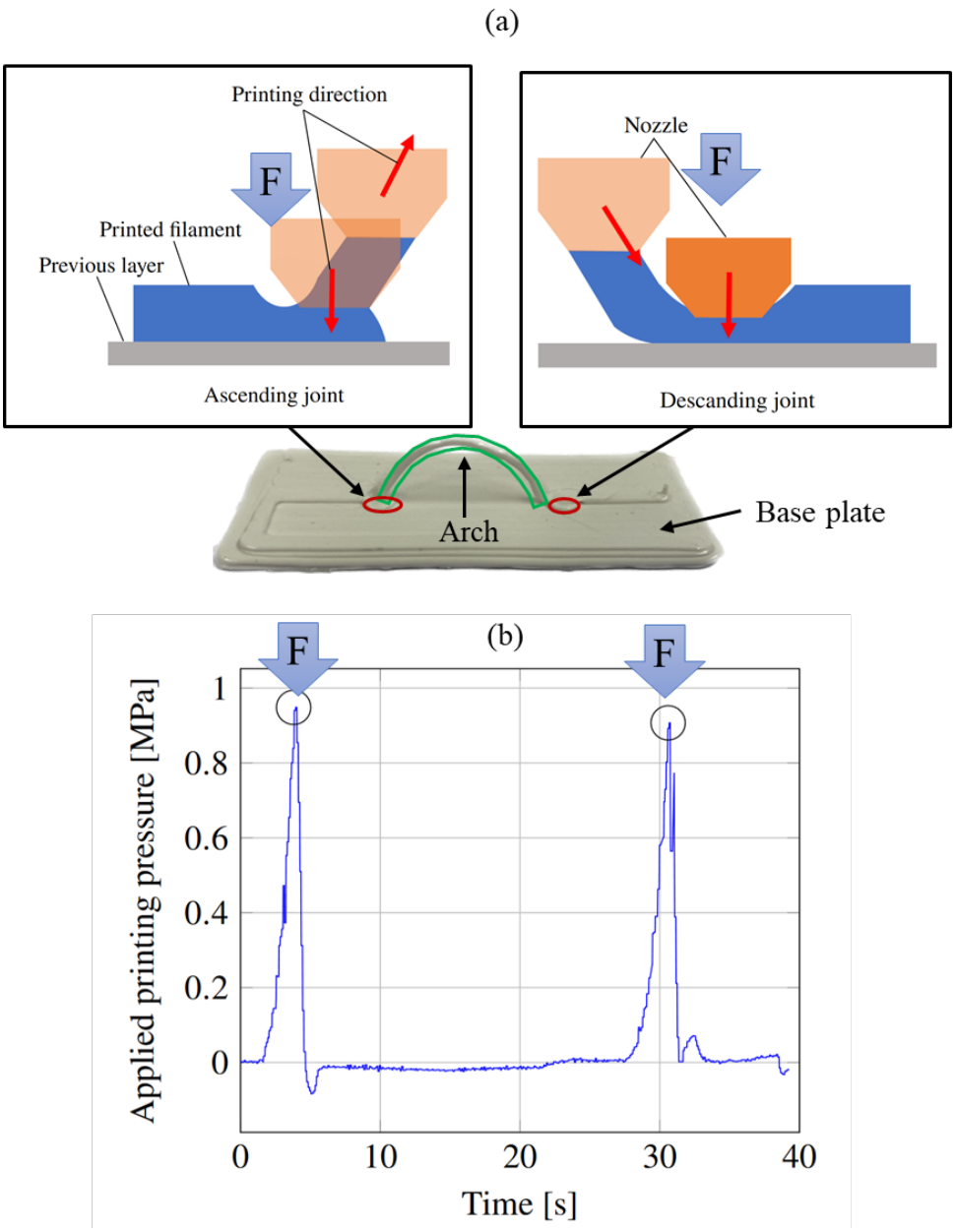

Fig. 5. Integrated force sensor used to (a) print arch structures and corresponding the nozzle trajectory during the ascending and descending trajectories, accordingly; and resulting (b) observed printing deposition pressure curve throughout the printing of the arch sample. The two peaks correlate with the induced pressures during the print.

During the tests, the specimens are pulled until failure, and the tensile force is recorded to determine the maximum load. A ZwickiLine Z1.0 universal testing machine from ZwickRoell is used as the testing apparatus. The specimens are attached, along with the base plate, to a stationary platform. A fastened hook is then inserted into the arch of the printed specimens to apply the tensile load. To avoid undue stress concentration between the hook and the arch, a curved metal plate with a smooth surface is positioned between the hook and the arch. This helps in increasing the contact area and distributing the applied load to the joints. A schematic illustration and an image of the testing setup and process is illustrated in Fig. 6.

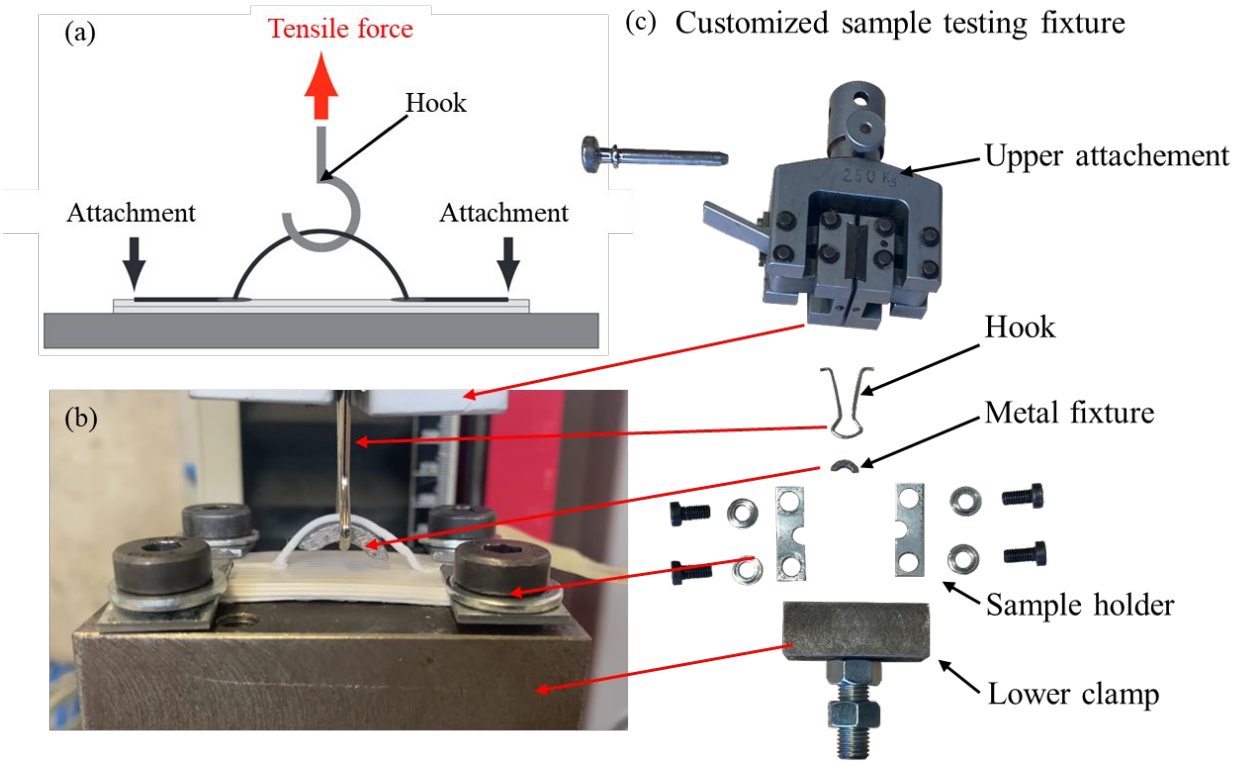

Fig 6. (a) schematic illustration and corresponding (b) actual depiction of the arch sample under the testing conditions, along with the (c) exploded view of the customized test fixture.

The test results are qualitatively analyzed by normalizing the recorded loads against the nozzle area (which ideally corresponds to the filament and joint cross-sectional areas). This approach generates a comparable value that indicates the overall strength of the joints in the arch.

Results and Discussion

Printing process

First, the performance of the adapted free-form fabrication process was assessed, especially upon integrating the force sensors and controlled deposition-pressure algorithms. Using the setup, upon incorporating the modified printing process with the offshoot movements and moderated extrusion rates, significant improvement within the manufactured truss elements was observed (See Fig. 7).

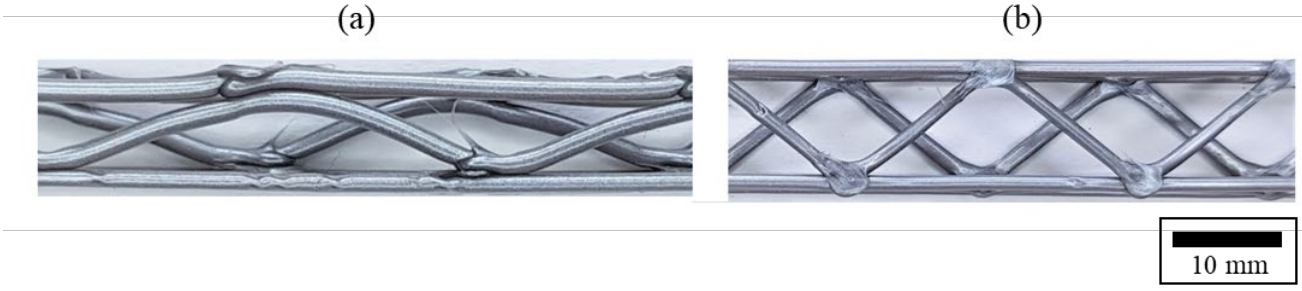

Fig. 7. Support-free truss structure 3D printed (a) without optimization and (b) with optimization.

Noticeably visible improvement in the support-free printed truss segment quality was observed (Fig. 7. b) when the optimized printing approach was incorporated, compared to the standard geometric G-code (Fig. 7. a)

without extrusion moderation. Symmetry across the segments, consistent link depositions, improved joint-connections, enable support-free printing of thermoplastic truss structures.

However, aesthetic improvement is insufficient to qualify the structure for functional applications. Therefore, the arch segments with varying nodal deposition pressures were printed for the tests, as illustrated in Fig. 5. Starting with 0 MPa of nodal pressure, with increments of 0.3 MPa up to 1.8 MPa, seven series of samples with varying nodal pressures were produced with a set of five samples for each series. The plot depicting the applied deposition pressure throughout the printing process for a sample with 0.9 MPa nodal pressure is illustrated in Fig. 5 b. These plots aid in assessing the robustness of our force-sensor integrated robotic printing apparatus, and the efficacy of our developed control algorithm to apply specific loads within designated sections of the prints. For the sensors, it was noted that the applied deposition pressure deviated less than 2.5 % of the input values. This deviation, although minuscule, is attributed to the discrepancy between the accuracy afforded by the robotic arm, and the integrated sensors.

Within the printed arches, it was observed that the sample arches would deviate further away from their optimal input shape, with the increase in deposition pressures. It was noticed that the application of nodal forces causes the nozzle to diverge at the nodes, offsetting away from the input geometric shape. With increased contact pressure, the contact surface at the joints was also observed to have increased. This was obvious as the nozzle would simultaneously extrude and apply the pressure at the node while dwelling on the position, leading to an increase in the contact area. The maximum deviation in printed samples geometries was within 14 % of the input geometric coordinates, with the discernible correlation being higher deposition pressure causes larger geometric deviation.

Tensile tests

The printed arch samples with varying nodal deposition pressures were subjected to the tensile tests as illustrated in Fig. 6. The following Fig. 8. summarizes the stresses at which the arches failed for corresponding deposition pressure. It must be noted that the contact areas and the geometries of the samples varied with the change in deposition pressure. The illustrated values in Fig. 8 b account for this deviation and are normalized against the contact area near the fractured surface to accurately evaluate the impact of deposition pressure on the strength of the joints.

From the plot in Fig. 8, it is apparent that there was an obvious increase in strength with increasing nodal deposition pressure. The trend follows a rectangular hyperbolic curve, meaning significantly higher breaking stress was observed for samples with a nominal increase in deposition pressure when compared to the sample without any induced deposition pressure. This increment however plateaus as the deposition pressure further increases. Qualitatively comparing the arch strength improvement, samples prepared with 1.8 MPa of nodal deposition pressure were over six times stronger than the samples prepared with no induced deposition pressure.

Additionally, two different types of failures were observed, viz. detachment at the joints and fracture within the arch (See Fig. 8 a). The detachment of the joints can be affiliated with peeling effect, as the printed arch structure would separate from the printed base plate. On the other hand, a fracture within the arch may not directly correlate with the failure of the joint. However, it can be hypothesized in these circumstances that the joint strength exceeded the strength of the arch segment. From a structural optimization perspective, it can be deemed as a success, since 3D printed support-free truss structures are prone to failure at the joints [13] and in this case, it no longer represents the critical failure point within the printed component.

Thus, concentrating our observations purely on nodal failure via detachment, we can assert that there is a positive correlation between the deposition pressure and the joint strengths at the nodes of 3D printed support-free truss structures. For samples manufactured using PLA, when the applied nodal deposition pressure is 1MPa, we observe a transitionary phase between the failure mode of the arch samples. At this phase, accounting only for joint strength improvement, the structures printed with nodal deposition pressure exhibited five times higher

strength than the structures with no induced deposition pressure. When the deposition pressure exceeds this threshold, the strength of the arch approaches the strength of the printed material itself (35 MPa), resulting in no significant improvement in arch strength thereafter.

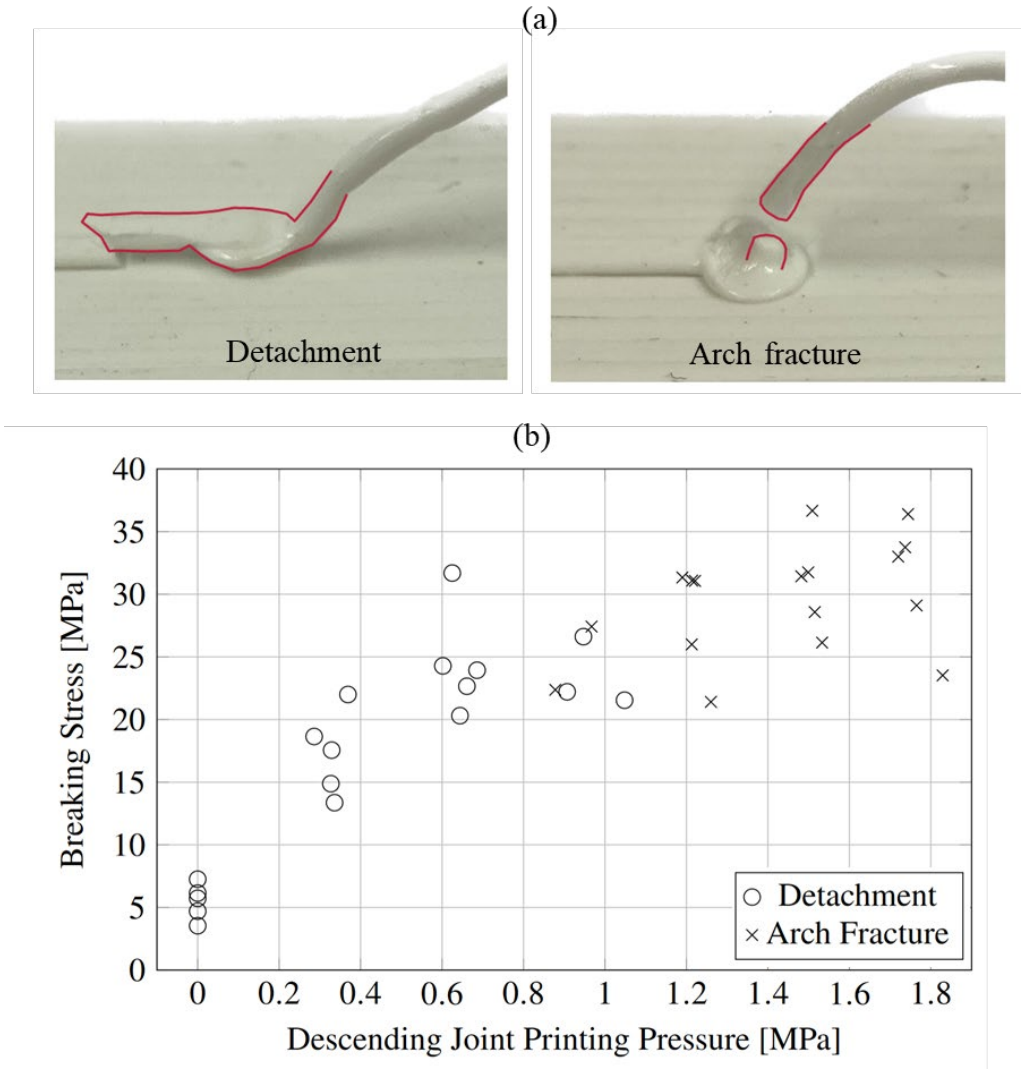

Fig. 8. (a) two different failure modes observed within arches: nodal detachment and arch fracture; (b) plot depicting breaking stresses vs. applied nodal deposition pressure and corresponding failure modes.

This improvement in the strength of the structure with the increase in the deposition pressure can be attributed to two identified factors:

- The applied pressure within FFF often helps in reducing the inherent air pockets, voids and inter-layer anomalies between the extrudes.
- For the demonstrated printing approach, an increase in deposition pressure also increases the dwell time of the hot end over the node. Thus, prolonging heat retention at the nodes, and improving interlayer adhesion.

From an optimization perspective, 1MPa of deposition pressure is critical when support-free 3D printing with the aforementioned printing apparatus and material combination. Applying 1MPa of nodal deposition pressure can be projected to ensure optimal structural strength within the printed truss. Within a free-flying environment, this assists in minimizing the impact of the resulting detrimental friction forces while printing with a mobile floating satellite module. Even with a nominally applied deposition force of 0.3 MPa, we observe over

three times higher strength, compared to samples without any induced nodal pressure. For terrestrial applications, the printing of functional multi-layered sparse structures can be made possible by fine-tuning the deposition forces, especially for the subsequent layers, without exerting excessive loads on previous layers.

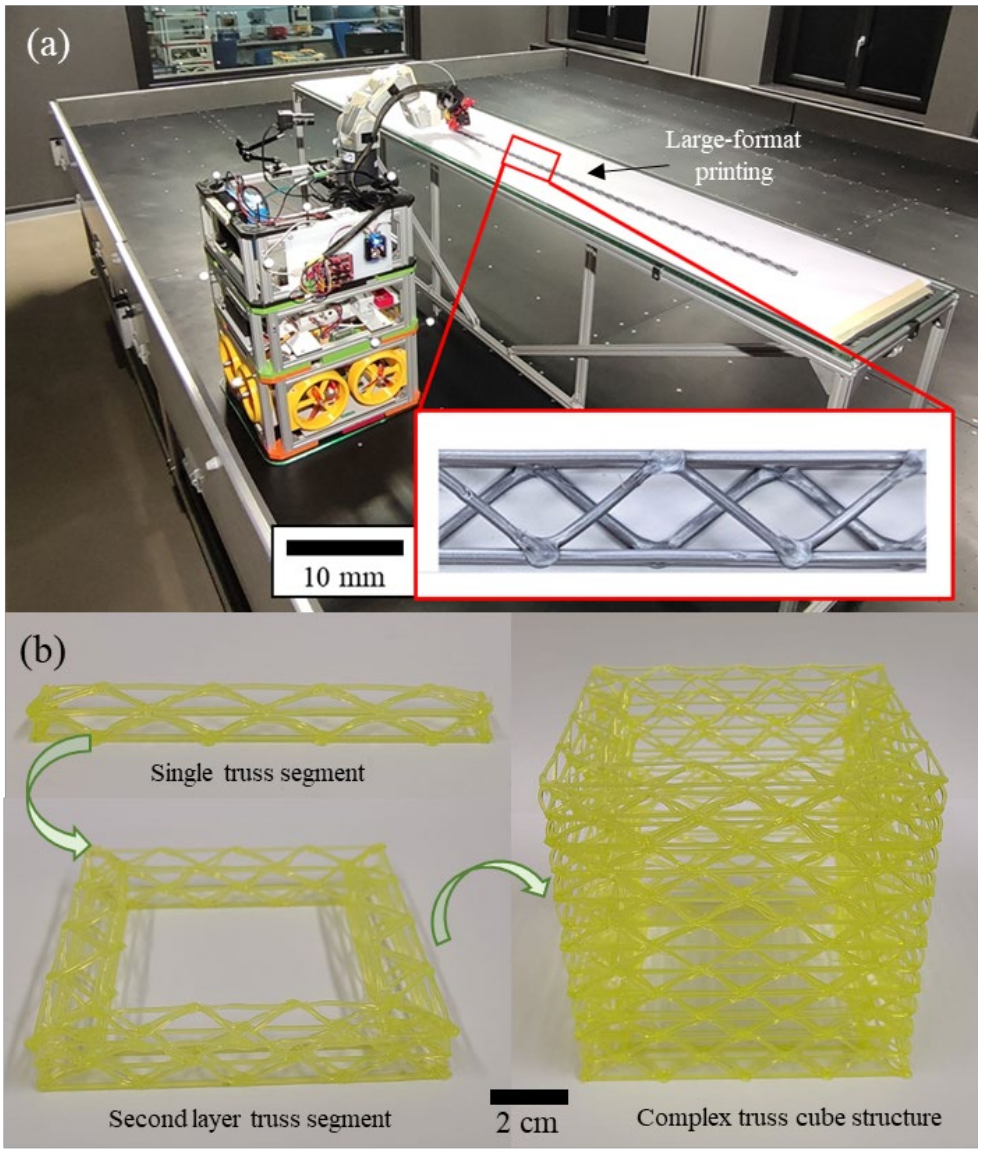

Fig. 9. (a) support-free printing of large-format trusses in space-simulated free-flying environment in ELISSA; (b) complex multi-layered support-free truss 3D printed using the robotic manipulator.

The findings of this parametric study were incorporated in both, space simulated as well as terrestrial environment. Within the ELISSA ecosystem, this integrated printing process exhibits immense potential in optimized printing of infinitely large continuous structures with uninterrupted tool-path (See Fig. 9. a). Within terrestrial free-form printing applications, structurally sound complex multilayered trusses can be successfully built by optimizing the deposition pressures within subsequent layers, without buckling the previous depositions (See Fig. 9. b)

Conclusion

In this study, a new development within ISM is presented. By integrating the pressure sensors within the robotic manipulator used for support-free printing, a parametric study was conducted that varied the deposition pressure during support-free printing. The sensors were programmed using an algorithm that dynamically modified the G-code to execute force-controlled joint commands. For the current setup, this facilitates dynamic deposition pressure control with over 97.5 % repeatable accuracy, as noted during arch printing experiment.

The parametrically induced pressure was correlated to its impact on the strength of the joints within the printed truss elements. A novel testing method was developed to quantify the variation in the strength of the joints which later facilitated in qualitative comparison between different printed structures.

The test results suggest a rectangular hyperbolic trend for the strength increase with an increase in deposition pressure. There is a positive correlation between deposition pressure and joint strength. However, this increment promptly plateaus after the deposition pressure exceeds 1 MPa for PLA structures. This trend coincides with the change in failure mode observed within the printed joints. Upon testing until failure, for the samples printed with deposition pressure less than 1 MPa, the arches detached from the base plate near the joints. For the samples printed with deposition pressure exceeding 1MPa, the fracture was observed in the arch itself, with measured strength coinciding with that of the PLA material itself. Thus, determining the ideal deposition pressure to ensure optimized join strength without generating excessive reaction forces.

This finding is particularly important when used to print large-format support-free structures in space-simulated free-flying environment. It aids in reducing the disturbances experienced by the free-flying mobile 3D printing platform. Thus, improving the overall printability afforded by the system, allowing for larger, more complex structures to be printed.

For terrestrial applications, other than multilayered lattice structure printing, the illustrated printing approach with integrated force feedback can facilitate printing on curved, uneven substrates by dynamically altering the G-codes. Thus, extending the field of application for 3D printing beyond specially prepared, dedicated substrates.

References

[1] Robert P. Hoyt. Spiderfab: An architecture for self-fabricating space systems. In AIAA SPACE 2013 Conference and Exposition, Reston, Virginia, 09102013. American Institute of Aeronautics and Astronautics.

[2] Wendel K. Belvin, William R. Doggett, Judith J. Watson, John T. Dorsey, Jay E. Warren, Thomas C. Jones, Erik E. Komendera, Troy Mann, and Lynn M. Bowman. In-space structural assembly: Applications and technology. 3rd AIAA Spacecraft Structures Conference, 2016.

[3] Niki Werkheiser. In-space manufacturing: Pioneering a sustainable path to mars.

[4] R. G. Clinton. Nasa's in space manufacturing initiative and additive manufacturing development and quality standards approach for rocket engine space flight hardware.

[5] Tracie Prater. Nasa's in-space manufacturing initiative: Initial results from international space station technology demonstration and future plans.

[6] Niki Werkheiser. Nasa additive manufacturing overview.

[7] Wei Gao, Yunbo Zhang, Diogo C. Nazzetta, Karthik Ramani, and Raymond J. Cipra. Revomaker: Functionally-embedded 3d printing using a rotational enabling multi-directional and cuboidal platform. In Celine Latulipe, Bjoern Hartmann, and Tovi Grossman, editors, Proceedings ofthe 28th Annual ACM Symposium on User Interface Software & Technology, pages 437–446, New York, NY, USA, 11052015. ACM.

[8] Xuan Song, Yayue Pan, and Yong Chen. Development of a low-cost parallel kinematic machine for multidirectional additive manufacturing. Journal of Manufacturing Science and Engineering, 137(2), 2015.

[9] Steven Keating and Neri Oxman. Compound fabrication: A multi-functional robotic platform for digital design and fabrication. Robotics and Computer-Integrated Manufacturing, 29(6):439– 448, 2013.

[10] Chenming Wu, Chengkai DAI, Fang Guoxin, Yong-Jin Liu, Charlie C.L. Wang. Robofdm: A robotic system for support-free fabrication using fdm. 2017 IEEE International Conference on Robotics and Automation (ICRA), 2017.

[11] Shuting Liu, Yingguang Li, and Nanya Li. A novel free-hanging 3d printing method for continuous carbon fiber reinforced thermoplastic lattice truss core structures. Materials & Design, 137:235–244, 2018.

[12] D. Jonckers, O. Tauscher, E. Stoll, and A. Thakur. Feasibility study of large-format, freeform 3d printing for on-orbit additive manufacturing. 2021 Solid Freeform Fabrication Symposium Proceedings (Austin, United States:, 2021.

[13] Declan Jonckers, Oliver Tauscher, Aditya R. Thakur, and Lasse Maywald. Additive manufacturing of large structures using free-flying satellites. Frontiers in Space Technologies, 3, 2022.

[14] Oliver Tauscher, Declan Jonckers, and Aditya R. Thakur. Algorithms for large scale additive manufacturing in a free-flying environment. Frontiers in Space Technologies, 3, 2022.

[15] Alberto Andreu, Sanglae Kim, Jörg Dittus, Marco Friedmann, Jürgen Fleischer, and Yong-Jin Yoon. Hybrid material extrusion 3d printing to strengthen interlayer adhesion through hot rolling. Additive Manufacturing, 55:102773, 2022.